Scientific Research Publishing

Chinese Studies, 2025, 14(2), 150-175
https://www.scirp.org/journal/chnstd
ISSN Online: 2168-541X
ISSN Print: 2168-5428

Chinese Porcelains of the Early 18th Century from the Commander Islands, Northwest Pacific: Archaeometry Study

Irina S. Zhushchikhovskaya[1], Igor Yu. Buravlev[2], Alexander A. Karpenko[3]

[1]Institute of History, Archaeology & Ethnology of Peoples of the Far East, Far Eastern Branch of the Russian Academy of Sciences, Vladivostok, Russia
[2]Institute of High Technologies and Advanced Materials, Far Eastern Federal University, Vladivostok, Russia
[3]A.V. Zhirmunsky National Scientific Center of Marine Biology, Far Eastern Branch of the Russian Academy of Sciences, Vladivostok, Russia
Email: irina1zh@mail.ru

How to cite this paper: Zhushchikhovskaya, I. S., Buravlev, I. Y., & Karpenko, A. A. (2025). Chinese Porcelains of the Early 18th Century from the Commander Islands, Northwest Pacific: Archaeometry Study. *Chinese Studies, 14,* 150-175.
https://doi.org/10.4236/chnstd.2025.142011

Received: April 1, 2025
Accepted: May 13, 2025
Published: May 16, 2025

Abstract

The article presents recent results derived from the study of a unique porcelain wares assemblage discovered during archaeological excavations of the site of the Commander Islands' temporary camp of the Great Northern Expedition headed by Vitus Bering. The camp was occupied in 1741-1742. The porcelain assemblage is small and fragmented, but it is interesting because of its varied and impressive decoration patterns, in particular, colorful painting. Preliminarily, the excavated wares were supposed to be Chinese production and date back to the early 18th century. The research goal is to interpret the porcelain assemblage based mostly on the wares' technological characteristics and using some methods of archaeometry adopted in modern studies of old Chinese porcelain. The obtained results confirm the Chinese origin of porcelain. It is revealed that the assemblage reflects some of the major trends in the development of Chinese porcelain technologies between the end of the 17th and early part of the 18th century. The considered assemblage contains the wares of the *Famille Rose*, *Famille Verte*, and *Powder Blue*, which are famous and valuable Chinese porcelain.

Keywords

Commander Islands, Vitus Bering, Archaeological Site, Porcelains, Methods of Archaeometry

1. Introduction

The late 17th and 18th centuries are known as the "Golden Age" of Chinese porce-

lain history. Outstanding technological and artistic innovations and developments took place in porcelain production during the Kangxi (1662-1722), Yongzheng (1723-1735), and Qianlong (1736-1795) periods of the Qing Dynasty (1644-1911). Large volumes of Chinese porcelain wares produced in government and private workshops were exported to European, Asian, and American markets (Harrison-Hall, 1997; Leath, 1999; Kerr & Wood, 2004: pp. 641-646, 745-747; Fang, 2010: pp. 94-118, 136-141; Colomban et al., 2022a; Wang & Yang, 2022). As a result, Chinese porcelain assemblages of the 18th century can be defined as expressions of global cultural heritage and are increasingly the focus of advanced archaeometry studies to better understand their technological characteristics. Special attention is directed at the analytical examination of the glazes, underglazes, and overglazes, which, in turn, largely determine the stylistic diversity of the porcelains (Miao et al., 2010; Colomban et al., 2020; Colomban et al., 2022b; Norris et al., 2022; Colomban et al., 2023).

The research focus of this article is a unique assemblage of Chinese porcelains excavated at the site of Vitus Bering's temporary camp at the Commander Islands in the Northern Pacific (**Figure 1**). This camp was the last refuge for the crew of the "St. Peter" sailing ship, one of two vessels of the Great Northern Expedition (1733-1742) headed by famous Danish and Russian seafarer, captain-commander Vitus Bering (1681-1741). After the ship was wrecked in early November of 1741, the crew of the boat were forced to seek refuge for no months on a remote island (known at present as Bering's Island). Using historical written sources and documents, archaeological investigations of campsites were conducted in 1979 and 1981. The excavations generated a rich and diverse collection of artifacts and utensils, among them, the series of broken and fragmented porcelain wares supposedly of Chinese origin (Len'kov et al., 1988; Len'kov et al., 1992).

Figure 1. Map of the research area—Northwest Pacific, Commander Islands (circled by red). (https://www.freeworldmaps.net/)

The porcelain assemblage recovered at Far Island in the Northwest Pacific is of certain scientific interest as a unique episode in the history of Chinese porcelains, which were starting to be traded globally by the early 18th century. The article presents the first attempt to study fragmented and discarded porcelain specimens based mostly on their technological features to compare with known sorts of Chi-

nese porcelain production from the late 17th to early 18th centuries. The methodological background is an archaeometry approach that includes a set of physicochemical methods.

2. Archaeological and Historical Context

Bering Island is the largest in the Commander Islands, located 175 kilometers east of the Kamchatka Peninsula in the Northwest Pacific. This island is 95 kilometers long and 15 kilometers wide; its area is 1667 square kilometers. The remains of V. Bering's temporary camp are located in Commander Bay on the northeastern coast among the sand dunes. Before the first field season in 1979, archaeologists found that cultural deposits of the camp remains had been disturbed earlier by non-professional excavations by amateurs. The investigations of V. Bering's campsite correspond to the scope of historical archaeology. The characteristic trait of the research strategy during the 1979 and 1981 seasons was that the archaeologists could correlate the fieldwork and their results with the data from writing sources containing information about the island wintering of 1741-1742. These sources are the Logbook, the Inventory List of the expedition's property, and the memoirs of some expedition members, in particular, of famous scientist Georg W. Steller (Len'kov et al., 1988: pp. 7-19).

According to the writing sources, after the forced landing, expedition members built six winter dwellings deep into the sandy ground at the seashore and, later, several ground dwellings for the summer season. During field seasons of 1979 and 1980, the remains of six temporary wintering pit-dwellings and two ground dwellings were recognized and unearthed. The total excavated area is about 1000 square meters. The depth of wintering dwellings' pits exceeded 1.0 m, sometimes reaching 2.0 m. In-pit dwellings and ground dwellings, numerous artifacts made of iron, bronze, copper, silver, glass, wood, leather, and ceramics were discovered. Among them, in particular, there were wooden containers for storage, metal cooking wares, several ceramic glazed pots and cups, and many fragmented and completed glass small-sized bottles. The fragments of porcelain wares were discovered inside the pit dwellings N1 and N5 and in the area of one ground dwelling near the pit-dwelling N2. No single completed item was unearthed. The Inventory List of the expedition's property included detailed registration of various instruments, navigation equipment, weapons, utensils, and other things. However, in the Inventory List, there were not any mentions of porcelain wares. (Len'kov et al., 1988: pp. 14-16). Based on that, the porcelains are supposed to be the personnel belongings of the ones of expedition members rather than some kind of expedition's property.

Beginning from the end of the 17th to early 18th century, Chinese porcelains, mainly table wares, regularly came to Russia. Porcelain was one of the categories of goods, together with tea, silk, and spices, imported from the Chinese Dynasty. At first, the goods arrived directly at trading markets in large Siberian cities, and then they moved to central regions of Russia, Moscow, and St-Petersborg. After 1728, the governments of the two great states reached an agreement on a perma-

nent trading route via the Kyakhta border post in southern Siberia, and the volumes of Chinese import goods increased significantly (Tataurov, 2017; Zagvazdina, 2017; Huang, 2019).

The years between 1733 and 1738 were the initial stages of the Great Northern Expedition when preparations for sea voyages across the Pacific from northeastern Siberia to America's north-western coast were conducted. During this period, many persons of the expedition commanding staff, and among them, captain-commander Vitus Bering, stayed briefly with their families in various eastern Siberian cities, including Tobolsk, Tyumen, and Yakutsk. It seems likely that the porcelains were purchased at Siberian markets in 1733-1738 and later were taken as personnel belongings to the Pacific voyage of 1740-1741.

3. Materials and Methods

In contrast to ancient porcelains stored under well-balanced conditions in the museums and private collections, our research materials, before they were unearthed, were buried for a long time in the cultural deposits of V. Bering's campsite. These were sandy soils saturated with various organic and non-organic remains. This certainly influenced the degree of preservation of fragile artifacts. When excavated, the porcelains were cleaned with water, and then some wares were restored partially by attaching and binding relevant fragments. Now, the collection of porcelains is stored in the Museum of Archaeology & Ethnography of the Institute of History, Archaeology & Ethnology of Peoples of the Far East, Far Eastern Branch of the Russian Academy of Sciences in Vladivostok.

The total assemblage consists of 13 broken items of tableware, including plates, saucer dishes, bowls, and cups, all numbered in this study as objects 1 - 13. The porcelains are of monochromic and polychromic color variants. The monochromic white is represented by object 1 covered with transparent colorless glaze. The monochromic blue is object 3 colored with the underglaze. Polychromic objects 4 - 13 exhibit a wide range of colored overglazes (**Figure 2(a)-(f)**; **Table 1**; **Table 2**).

A distinctive feature of objects 4 and 6 is the presence of trading marks at the outer bottom surfaces. The mark at object 4 represents six blue-colored hieroglyphs forming two vertical rows within a double circle (**Figure 2(g)**). This is a well-known porcelain reign mark, meaning that the artifact was produced during the Yongzheng period of the Great Qing Dynasty. The bottom mark at object 6 decorated with gold flower composition (**Table 1**), is a blue-colored drawing image within a double circle (**Figure 2(h)**). This kind of symbolic marking is known from the Kangxi period. The image consisting of brush for the calligraphy (*pi*), a cake of ink (*ting*), and a scepter of longevity (*ju'i*) makes the rebus *Pi ting ju'i* meaning "May (things) be fixed as you wish!" (Burton & Hobson, 1909: pp. 136, 141).

The research methods applied in this study include visual observation, optical microscopy, SEM-EDS examination, portable XRF examination, and Raman spectroscopy, which are aimed at identifying the textural and compositional features of the porcelains. Taking into account the uniqueness and significant scien-

tific value of porcelain assemblage from V. Bering's campsite, all methods used in the project are non-destructive.

Figure 2. Examined porcelains (selected specimens): (a) object 3; (b) object 4; (c) object 9; (d) object 7; (e) object 8; (f) object 11; (g) object 4, bottom outside; (h) object 6, bottom outside.

Table 1. List of the porcelain assemblage's objects.

Ware/Object N	Image	Shape Type	Condition	Size
1		Plate	Restored partially (mouth part)	Mouth diameter (appr. 16.7 cm)
2		Non-Detected	Fragmented	Non-Detected

Continued

3		Bowl	Fragmented	Mouth diameter (appr. 16.5 cm) Bottom diameter (appr. 12 cm)
4		Saucer Dish or Small Plate	Restored Partially	Bottom diameter (8.7 cm) Mouth diameter (appr. 17.5 cm)
5		Plate	Restored partially (bottom part)	Bottom diameter (appr. 8.7 cm)
6		Plate	Restored partially (bottom and mouth parts)	Bottom diameter (appr. 9.0 cm)
7		Saucer-Dish or Small Plate (Bottom and Rim Parts)	Restored partially	Bottom diameter (appr. 6.8 cm)
8		Saucer-Dish or Small Plate	Restored partially	Bottom diameter (appr. 8.0 cm)
9		Bowl	Fragmented	Mouth diameter (appr. 11 cm)

Continued

10		Cup	Restored partially	Mouth diameter (appr. 6.8 cm)
11		Bowl-like	Single fragment	Non-Detected
12		Bowl	Restored partially	Mouth diameter (appr. 10.5 cm) Bottom diameter (6.9 cm)
13		Non-Detected	Fragmented	non-detected

Table 2. List of underglazes and overglazes analyzed areas.

Layer	Color	Object N	Analyzed Area, Site	Applied Methods
Underglaze	Blue	3		SEM-EDS pXRF
		4 (bottom mark)	 site 1 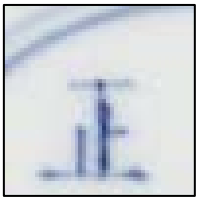 site 2	pXRF
		6 (bottom mark)		pXRF

Continued

Overglaze/Enamel	Blue	7		pXRF
		8		Raman pXRF
		10		SEM-EDS
	Yellow	4	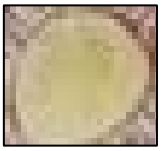	Raman pXRF
	Emerald-green (“cold” green)	4		pXRF
		9		SEM-EDS
	Grass-green (“warm” green)	4		pXRF
		9		SEM-EDS
	Terracotta-red	8		Raman pXRF
		4	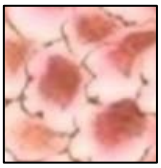	Raman pXRF

Continued

	5		SEM-EDS
Vermeil-red	6		SEM-EDS
Brown-black	7		Raman SEM-EDS
Violet-pink	13		SEM-EDS
Turquoise-blue	13		SEM-EDS
White	10		SEM-EDS
Ruby-pink	10		SEM-EDS pXRF
	11		SEM-EDS pXRF
Gold	6		SEM-EDS pXRF

Visual observation equipped with magnifying glass was purposed to study macro-features of body texture, glazes and overglazes, or enamels, the details of painting. The equipment used is a portable magnifying glass TH-7015 Kromatech, with an observed area diameter of 6.5 cm and magnification of 10x. Optical microscopy (OM) was applied to determine the textural characteristics of the porcelain's body, glaze, underglaze, and overglaze layers in surface and cross-section positions (Colomban et al., 2017; Colomban et al., 2022c). The used equipment is an inverted Carl Zeiss Axiovert 40 MAT microscope, assembled with a digital AxioCam ERc 5 s camera (Carl Zeiss Microimaging GmbH production Germany), with a magnification range of 10 - 1000×. The equipment is not fitted for work with objects of complex configuration and curved surfaces. The selected objects 2, 3, 5, 6, 8, 9, 11, and 13 were examined under the magnification 50× in surface and cross-section positions. It has to be noted that previously restored objects 5, 6, and 8 were unglued for the sampling and examination and then reglued. The optical microphotographs of surfaces and cross-sections are presented in **Figure 3**.

The X-ray fluorescence spectroscopy, in particular, portable XRF, and electron scanning microscopy combined with energy-dispersive spectroscopy (SEM-EDS) are applied to determine the porcelain's bodies, glazes, underglazes, and overglazes elemental compositions (Norris et al., 2020; Norris et al., 2022; Colomban et al., 2022b; Colomban et al., 2022c; Colomban et al., 2023). The pXRF equipment used in our research project is the fluorescence spectrometer of the model Olympus Delta Professional DP 4000, which analyses a surface area up to 10 mm in diameter and provides approximate average quantitative data on the content of chemical elements (in % wt.). The analyzer instrument calibrated with a standard Olympus Analytical Instrument 316 operates in the metal detecting regime with limitations in the diagnostic capabilities for elements whose atomic weight is less than 44, specifically concerning N, Ca, the alkalis K, Na, Mg, the As, and some others. The pXRF testing was conducted for objects 3, 4, 6, 8, 9, 10, and 11 to examine the body, underglazes and overglazes compositions. The analyzed areas of underglazes and overglazes are presented in **Table 2.** Measurements were taken in an air atmosphere through a PRO 6 Prolen U8990460 (6 μm) window in dual beam mode for 40 s (10 s, 30 s). Considering the limited diagnostic possibilities and approximate nature of quantitative data, the detected elements are considered major, minor, and trace in qualitative evaluation. The results are summarized in **Table 3**.

Raman spectroscopy was employed in this study to determine the mineral phases composition of porcelains' glazes and overglazes (Miao et al., 2010; Colomban et al., 2017; Colomban et al., 2020; Colomban et al., 2022a). Analytical equipment is an InVia Reflex Raman micro-spectrometer (Renishaw, United Kingdom) coupled with a Leica DM2500 M universal microscope (at incident light mode: Leica Microsystems, Germany). For excitation, a 532 nm diode-pumped laser at a power of 1.0 mW and exposure time of 0.1 s was used, and 100 - 200 scans were used. A laser spot with a diameter of ~2 μm on the sample was formed with a lens (20×,

NA = 0.4, Leica). Laser power, total measuring time, and number of accumulations were set to obtain good signal-to-noise ratios. The spectra were processed using smooth baseline subtraction and peak fit functions in the WiRE 4.4 software. The spectrum of each sample at each location (three locations per sample) was measured over a range of 170 to 1800 cm^{-1}. Raman spectroscopy was applied to objects 4, 7, and 8 to test the yellow, red, brown-black, and blue overglazes. The results are presented in Figure 4.

The SEM-EDS machine used in our project is a ZEISS scanning electron microscope EVO-40 (Oberkochen, Germany) equipped with the energy dispersive spectrometer (EDS) of the Oxford Instruments INCA-x sight. The acceleration voltage of the SEM examination was kept at 20 kV; the working distance was held at 13.0 - 16.5 mm; and the magnification regime was 500 - 1000×. The sampling box of the equipment is designed for the testing of relatively small and simply shaped objects. Objects 9,11, and 13 and the sampled fragments of objects 1, 3, 5, 6, and 10 sufficient to put into the camera were analyzed to investigate glaze, underglaze, and overglaze compositions. The measurements were provided on unpolished surfaces without special films or coatings (carbon, chromium, or gold). The analyzed areas are presented in Table 2. The number of testing spots for one object/sample is 2 - 4, and the number of EDS spectra taken at one spot is 15 - 16. The compositions of selected EDS spectra converted in the oxide form are summarized in Table 4. Selected SEM images are presented in Figure 5.

4. Research Results

In this section, the textural and compositional features of the bodies, glazes, underglazes, and overglazes are considered.

4.1. Bodies

The thickness of the porcelain items' walls and bottom fragments ranges from 1.5 to 2.2 mm. Macroscopically, the cross-sections demonstrate the homogenous texture and white color of the body, sometimes with a light yellowish or grayish tone. Optical microscopy of the unpolished cross sections indicates that the body layer contains black, brown, or yellowish inclusions of irregular shapes and variable size (Figure 3(a)-(g)). These are likely the result of soil pollution caused by the long-term burial of the porcelain.

The fractured unpolished sections of objects 3 and 4 were examined with the pXRF (Table 3). The SEM-EDS examinations could not be provided without the destruction of porcelain fragments. The pXRF detected Si and Al as the main elements. Fe is recognized as a minor element that may be the result of porcelain surface pollution with ferric ions from the soil. For the body of object 3, a distinctive feature is the presence of Mn as a minor element and Co as a trace element. As shown below, Mn and Co are important components of blue underglaze decoration laying over the porcelain body of the ware 3. Taking into account the specificity of the pXRF testing procedure, the signals of these elements cannot be at-

tributed to the porcelain body as such. Testing site 1 at object 4 showed Pb as a minor element. The lead could penetrate into transparent glaze from lying above colored overglazes or enamels. The researchers emphasize the high volatility and fluidity of the lead above 900˚C (Colomban et al., 2017).

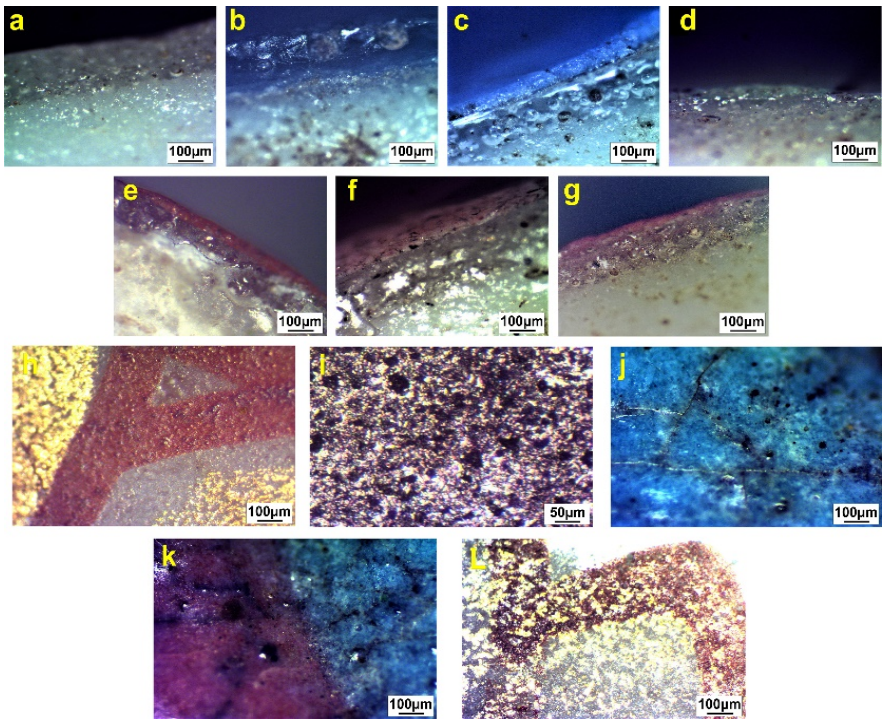

Figure 3. Optical microphotographs. Cross sections: (a) object 1; (b) object 3; (c) object 10; (d) object 9; (e) object 5; (f) object 13; (g) object 11. Surfaces: (h) object 5; (i) object 7; (j) object 13; (k) object 13; (l) object 6.

Table 3. Chemical elements detected with pXRF in the body, underglaze, and overglaze layers.

Layer	Object N/spot	Color	Elements (**major**-minor-*trace*)
Body	3/1		**Si**, **Al**, Fe, Mn, *P*, *Co*, *Zn*, *S*
	4/1		**Si**, **Al**, Fe, P, *Pb*, *Mn*
	4/2		**Si**, **Al**, Fe, Pb, *Mn*, *P*, *S*
Underglaze	3/1	Blue dark	**Si**, **Al**, **Mn**, Fe, Co, *Zn*, *Ni*
	3/2	Blue light	**Si**, **Al**, Mn, Fe, Co, *Ni*
	4 bottom/1	Blue	**Si**, **Al**, Fe, Mn, S, *Co*, *P*
	4 bottom/2	Blue	**Si**, **Al**, Fe, Mn, S, *Co*, *P*
	6 bottom/1	Blue	**Si**, **Al**, Fe, Mn, S, *Co*, *P*, *Pb*

Continued

	7	Blue	**Si**, **Pb**, **Al**, Fe, *Co*, *Mn*, *P*, *Bi*, *Ni*, *Cu*
	8	Blue	**Si**, **Pb**, **Al**, Fe, Au, Hf, P, *Co*, *Mn*, *Ni*, *Zr*
	4	Emerald-Green	**Si**, **Pb**, Al, Cu, Fe, *Sb*, *Mn*
	4	Grass-Green	**Si**, **Pb**, **Al**, Fe, Sn, Cu, *Mn*
Overglaze	4	Yellow	**Si**, **Pb**, Al, Fe, Sn, Hf, *P*, *Re*, *Mn*, *Zr*, *Ni*
	4	Terracotta-red	**Si**, **Pb**, Al, Fe, P, *Zn*, *Mn*
	10	Ruby-pink	**Si**, **Pb**, Al, Fe, P, *Au*, *Zn*, *Mn*, *Cu*
	11	Ruby-pink	**Si**, **Pb**, Al, Fe, P, *Au*, *Zn*, *Mn*
	6	Gold	**Au**, **Si**, **P**, Pb, Al, Fe, Ag, *Mn*, *Bi*, *Zr*

Note: **Major element** ≥ 10.0% wt. Minor element ≥ 1.0% wt. *Trace element* less than 1.0% wt.

4.2. Glazes

Colorless transparent glaze lying over the body at monochromic white object 1 and polychromic overglazed objects 5, 9, 10, 11, 13 varies in thickness from 150 to 350 μm (**Figure 3(a)**, **Figures 3(c)-(g)**). At the monochromic object 3, the glaze layer lying over the colored blue layer is 100 - 150 μm thick (**Figure 3(b)**).

The SEM-EDS testing conducted for objects 1, 6, and 13 shows strong composition uniformity (**Table 4**). SiO_2 and Al_2O_3 are recognized as the major components in ratios 4.7 - 5.7, and minor elements are K_2O, Na_2O, and CaO. The composition of transparent glaze at tested objects may be associated with quartz-feldspar glazes containing alkalis and lime (Kerr & Wood, 2004: pp. 560-562). Raman examination of object 4 in the colorless glazed area (**Figure 4(a)**) detects a highly shifted peak at 460 cm^{-1} and peak at 502 cm^{-1} associated with the dissolved quartz and feldspar grains, respectively, in the colorless glaze. The peak at 485 cm^{-1} corresponds to the glassy aluminosilicate phase, also recognized in colorless glazes (Colomban et al., 2017; Colomban et al., 2020).

Table 4. The data of selected SEM-EDS spectra (normalized) of glaze, underglaze, and overglaze layers. In the oxides wt%.

Layer	Color	Object-site-*testing spot*	Na_2O	MgO	SiO_2	Al_2O_3	P_2O_5	K_2O	CaO	TiO_2	MnO	Fe_2O_3	CoO	CuO	NiO	BaO	As_2O_5	SnO_2	PbO	Cl	N	Au	Ag
Glaze	Colorless transparent	1-1-*1*	1.7	nd	**63.4**	**13.5**	nd	3.3	2.5	nd	nd	1.7	nd	nd	nd	nd	nd	nd	nd	nd	nd	nd	nd
		1-1-*2*	1.5	nd	**63.5**	**13.1**	nd	3.3	2.4	nd	nd	1.5	nd	nd	nd	nd	nd	nd	nd	nd	nd	nd	nd
		1-1-*3*	1.6	nd	**63.7**	**13.5**	nd	3.2	2.5	nd	nd	1.6	nd	nd	nd	nd	nd	nd	nd	nd	nd	nd	nd
		6-1-*1*	3.1	nd	**64.7**	**11.4**	nd	3.6	1	nd	nd	3.1	nd	nd	nd	nd	nd	nd	nd	nd	nd	nd	nd
		6-1-*2*	2.9	nd	**62.5**	**12.5**	nd	3.6	1.4	nd	nd	2.9	nd	nd	nd	nd	nd	nd	nd	nd	nd	nd	nd
		6-1-*3*	3	nd	**61.8**	**13.2**	nd	3.4	1.5	nd	nd	3	nd	nd	nd	nd	nd	nd	nd	nd	nd	nd	nd
		13-3-*1*	2.1	nd	**61.8**	**12.8**	nd	3.8	2.2	nd	nd	2.1	nd	nd	nd	nd	nd	nd	nd	nd	nd	nd	nd

Continued

		13-3-*2*	2	nd	**61.8**	**12**	nd	3.9	2.1	nd	nd	2	nd	nd	nd	nd	nd	nd	nd	nd	nd	nd
		13-3-*3*	2	nd	**61.8**	**12.1**	nd	3.9	2	nd	nd	2	nd	nd	nd	nd	nd	nd	nd	nd	nd	nd
Underglaze	Dark blue	3-1-*1*	3.0	nd	**63.4**	**10.7**	nd	4.1	3.1	nd	3.9	1.9	*0.6*	nd	nd	nd	nd	nd	nd	nd	nd	nd
		3-1-*2*	3.4	nd	**60.9**	**10.9**	nd	3.4	2.6	nd	3.1	1.8	*0.6*	nd	nd	nd	nd	nd	nd	nd	nd	nd
		3-1-*3*	2.8	nd	**61.1**	**11.2**	nd	3.3	2.7	nd	3.4	2.0	*0.6*	nd	nd	nd	nd	nd	nd	nd	nd	nd
	Light blue	3-1-*1*	2.6	nd	**67.7**	9.1	nd	3.3	2.6	nd	1.5	1.4	*0.3*	nd	nd	nd	nd	nd	nd	nd	nd	nd
		3-1-*2*	1.6	nd	**64.5**	**10.7**	nd	3.1	3.6	nd	2.1	1.9	*0.3*	nd	nd	nd	nd	nd	nd	nd	nd	nd
		3-1-*3*	*0.9*	nd	**76.6**	5.5	nd	1.6	1.9	nd	0.9	1.0	n/d	nd	nd	nd	nd	nd	nd	nd	nd	nd
Overglaze	Blue	10-1-*1*	1.3	nd	**41.3**	*0.7*	nd	5.1	nd	nd	nd	*0.6*	*0.6*	nd	nd	*0.7*	1.3	nd	**24**	*0.4*	nd	nd	nd
		10-1-*2*	1.2	nd	**40.0**	*0.6*	nd	5.5	nd	nd	nd	*0.5*	*0.5*	nd	nd	n/d	1.4	nd	**25.4**	*0.3*	nd	nd	nd
		10-1-*3*	1.3	nd	**39.4**	*0.7*	nd	5.01	nd	nd	nd	*0.5*	*0.7*	nd	nd	*0.8*	1.1	nd	**24.6**	*0.3*	nd	nd	nd
	Grass-green	9-1-*1*	*0.7*	n/d	**34.9**	*0.5*	nd	nd	nd	nd	nd	*0.5*	nd	*0.8*	nd	nd	nd	**12.0**	**28.8**	*0.4*	nd	nd	nd
		9-1-*2*	*0.7*	n/d	**31.6**	*0.6*	nd	nd	nd	nd	nd	*0.6*	nd	*0.4*	nd	nd	nd	**36.9**	2.4	*0.3*	nd	nd	nd
	Emerald-green	9-2-*1*	*0.7*	nd	**56.0**	*0.7*	nd	1.4	n/d	nd	nd	n/d	nd	**2.1**	nd	nd	nd	nd	**14.8**	*0.5*	nd	nd	nd
		9-2-*2*	*0.6*	nd	**57.2**	*0.7*	nd	1.2	*0.2*	nd	nd	0.3	nd	**2.0**	nd	nd	nd	nd	**11.4**	*0.5*	nd	nd	nd
		9-2-*3*	*0.7*	nd	**58.9**	*0.8*	nd	1.4	n/d	nd	nd	n/d	nd	**1.9**	nd	nd	nd	nd	**14.1**	*0.6*	nd	nd	nd
	Terracotta-red	5-1-*1*	1.1	nd	**24.1**	4.5	nd	*0.7*	1.1	nd	nd	**16**	nd	nd	nd	nd	nd	nd	**24.8**	nd	nd	nd	nd
		5-1-*2*	1	nd	**25.7**	4.5	nd	*0.7*	1.3	nd	nd	**15.4**	nd	nd	nd	nd	nd	nd	**26.3**	nd	nd	nd	nd
		5-1-*3*	1	nd	**25.8**	4.5	nd	*0.6*	1.4	nd	nd	**15**	nd	nd	nd	nd	nd	nd	**26.1**	nd	nd	nd	nd
	Vermeil-red	6-1-*1*	1.3	*0.2*	**26.1**	5.2	nd	1.3	2.2	nd	0.1	**13.9**	nd	*0.3*	nd	nd	nd	nd	**13.9**	*0.1*	nd	*0.5*	*0.5*
		6-1-*2*	1.4	*0.3*	**24.2**	4.8	nd	1.1	2.3	nd	nd	**22.9**	nd	*0.9*	nd	nd	nd	nd	**14.1**	nd	nd	nd	nd
		6-1-*3*	1.4	nd	**29.8**	5.7	nd	1.4	2.7	nd	nd	**13.2**	nd	*0.5*	nd	nd	nd	nd	**18.2**	nd	nd	nd	*0.7*
	Violet-pink	13-1-*1*	1.0	*0.2*	**28.9**	4.5	nd	3.1	1.4	nd	1.0	1.3	nd	nd	nd	nd	nd	nd	**10.4**	*0.2*	nd	nd	nd
		13-1-*2*	1.0	n/d	**37.3**	4.4	nd	4.1	1.4	nd	1.3	1.1	nd	*0.9*	nd	nd	nd	nd	**17**	nd	nd	nd	nd
		13-1-*3*	*0.8*	n/d	**23.3**	4.1	nd	3.1	1.0	nd	*0.5*	1.1	nd	nd	nd	nd	nd	nd	4.1	*0.2*	nd	nd	nd
	Brown-black	7-1-*1*	1.5	nd	**11.9**	4	*0.7*	1.1	1.1	n/d	n/d	**29.7**	nd	nd	nd	nd	nd	nd	**11.1**	*0.3*	nd	nd	nd
		7-1-*2*	*0.8*	nd	8.8	3	*0.5*	1.1	1.5	n/d	*0.3*	**35.5**	nd	nd	nd	nd	nd	nd	**17.2**	*0.4*	*0.9*	nd	nd
		7-1-*3*	1.1	nd	**10.7**	3.3	*0.7*	1.2	1.9	0.4	*0.5*	**25.7**	nd	nd	nd	nd	nd	nd	**21.2**	*0.5*	nd	nd	nd
	White	10-3-*1*	*0.9*	nd	**33.4**	*0.7*	nd	2.9	nd	nd	nd	nd	nd	nd	nd	nd	4.2	nd	**26.1**	*0.6*	nd	nd	nd
		10-3-*2*	1.0	nd	**31.7**	*0.5*	nd	3.8	nd	nd	nd	nd	nd	nd	nd	nd	3.8	nd	**34.6**	*0.7*	nd	nd	nd
		10-3-*3*	1.0	nd	**29.6**	*0.6*	nd	3.8	nd	nd	nd	nd	nd	nd	nd	nd	3.7	nd	**31.2**	*0.7*	nd	nd	nd
	Turquoise-blue	13-*1*	*0.6*	nd	**34.2**	*0.7*	nd	3.2	nd	nd	nd	nd	1.5	nd	nd	nd	2.4	nd	**35.0**	nd	nd	nd	nd
		13-*2*	*0.4*	nd	**27.5**	*0.7*	nd	4.7	nd	nd	nd	nd	3.5	nd	nd	nd	1.2	nd	**36.5**	nd	nd	nd	nd
		13-*3*	*0.6*	nd	**34.2**	*0.7*	nd	3.2	nd	nd	nd	nd	1.6	nd	nd	nd	2.0	nd	**37.1**	nd	3.1	nd	nd
	Ruby-pink	11-1-*1*	*0.7*	nd	**41.8**	*0.7*	*0.9*	2.7	nd	nd	nd	*0.3*	nd	nd	nd	nd	nd	nd	**11.1**	*0.5*	nd	nd	nd
		11-1-*2*	*0.4*	nd	**44.9**	*0.5*	nd	4.4	nd	nd	nd	nd	nd	nd	nd	nd	nd	nd	**22.3**	*0.5*	nd	nd	nd
		11-1-*3*	*0.5*	nd	**52.9**	*0.8*	nd	5.02	nd	nd	nd	nd	nd	nd	nd	nd	nd	nd	**25.4**	*0.8*	nd	nd	nd
	Gold	6-2-*1*	1.2	*0.2*	**18.4**	3.4	nd	*0.8*	1.3	nd	nd	*0.6*	nd	nd	nd	nd	nd	nd	**14.5**	nd	2.3	**19**	3.9
		6-2-*2*	nd	nd	1.6	*0.8*	nd	nd	*0.4*	nd	nd	*0.5*	nd	nd	nd	nd	nd	nd	nd	nd	9.4	**46.7**	**10.8**
		6-2-*3*	nd	nd	2.9	*0.8*	nd	nd	*0.5*	nd	nd	*0.4*	nd	nd	nd	nd	nd	nd	nd	nd	6.3	**60.7**	**12.5**

Note: Au and Ag are presented as metals wt%; Cl and N are elements wt%. **Major element** ≥ 10.0% wt. Minor element ≥ 1.0% wt. *Trace element* less than 1.0% wt. CO_2 wt% is not included.

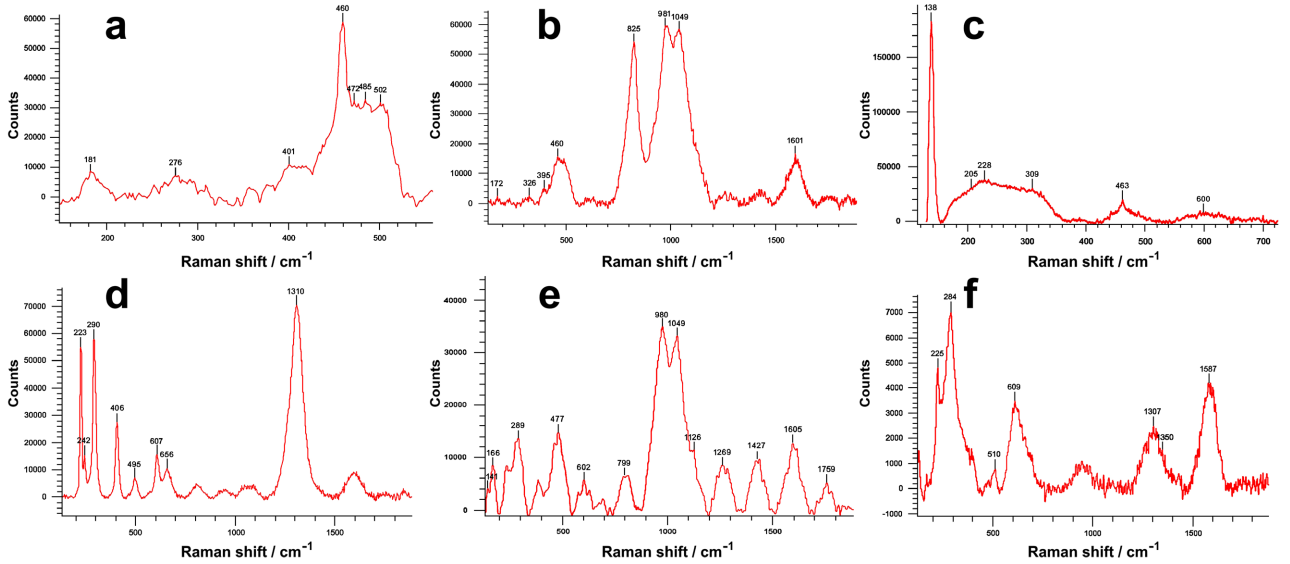

Figure 4. Raman spectra recorded: (a) object 4, colorless glaze; (b) object 8, blue overglaze; (c) object 4, yellow overglaze; (d) object 8, terracotta-red overglaze; (e) object 4, terracotta-red overglaze; (f) object 7, brown-black overglaze.

4.3. Underglazes

The blue-colored underglazes are registered on object 3 as exterior and interior surface decoration and on objects 4 and 6 as bottom markings.

One characteristic trait of object 3 underglaze is the uneven color and spotted appearance of dark blue and light blue areas (**Figure 2(a)**; **Table 2**). The optical microscopy of the cross-section shows the sequence of the layers: body matrix, underglaze blue, and surfaced colorless glaze. The thickness of the blue-colored underglaze layer, looking relatively dense and uniform in its texture, is around 70 - 100 μm (**Figure 3(b)**).

The pXRF and SEM-EDS examinations were provided in dark-colored and light-colored blue areas at one of the object's fragments. Taking into account the technical conditions of spectra testing, it is clear that the results reflect summarized data on the upper colorless glaze layer and the blue underglaze beneath (**Table 3**; **Table 4**). The content of Si and Al seems to be due to the composition of the upper layer of transparent glaze to some degree. The pXRF indicates the Mn, Fe, and Co in dark and light blue areas. Mn in dark areas is a major element (**Table 3**). It may be noted that Mn concentrations in dark and light areas are around 5 - 6 times higher than the Co concentrations. The SEM-EDS detects MnO and Fe_2O_3 as minor elements and CoO as a trace element in both areas. The concentrations of MnO are around 5 - 7 times higher than CoO ones in both areas, while in dark areas, the MnO and CoO are higher than in light ones (**Table 4**). Blue underglaze bottom marks were examined with the pXRF at two spots of object 4 and one spot of object 6. Major elements are Si and Al in similar concentrations for both objects. Mn and Fe are detected as minor elements, and Co as the trace one (**Table 3**). The concentrations of Mn are 6 - 7 times higher than the Co concentrations.

4.4. Overglazes

Colored overglazes are identified on objects 4 - 13. The distinctive colors are blue, yellow, green, terracotta-red, vermeil-red, brown-black, violet, violet-pink, turquoise-blue, turquoise-green, white, ruby-pink, and gold paint. All overglazes, excluding the green tones on objects 4, 5, 9, and 12, have an opaque appearance. The green overglazes, in contrast, look transparent and viscous. Two main techniques of overglaze application are distinguished preliminary—the painting, or brushing, and the drawing. The last produces fine lines of 0.2-0.3 mm width used as the contouring, bordering, or accenting elements in the pictured composition. Under the optical microscope, the lines look very accurate, well-defined, and applied, probably with some kind of stencil (**Figure 3(h)**). In this study, attention is mainly focused on the painted overglazes. Most of the recognized color variants were examined to determine textural and compositional features.

1) Blue

Blue-colored overglazes are presented at the objects 4, 7, 8, and 10 (**Figure 2(b)**, **Figure 2(d)**, **Figure 2(e)**; **Table 1**; **Table 2**). Optical microscopy of object 10 cross-section detected the sequence of the layers: body matrix, transparent glaze, and blue overglaze of 70 - 100 μm thick (**Figure 3(c)**). The elemental composition of blue overglaze is determined at objects 7 and 8 by the pXRF and at object 10 by the SEM-EDS. The pXRF detected Si, Pb, and Al as major elements, Fe as minor elements, and Co and Mn as trace elements in almost equal concentrations. The presence of Cu in object 7 is obviously caused by the quiet bordering of the tested blue area to the area painted with turquoise-green overglaze. The same situation is for object 8 where blue-painted and gold-painted areas are in touch, causing the Au as a minor element (**Table 3**). The EDS data for object 10 show high SiO_2 and PbO, as well as minor As_2O_3 and K_2O. CoO and Fe_2O_3 are detected in equal trace concentrations. The MnO is not signed. The distinctive trait of EDS spectra of blue overglaze is BaO as a trace (**Table 4**). The results of Raman spectroscopy applied to the blue overglaze at object 8 are presented in **Figure 4(b)**. The intensive peak at 825 cm^{-1} is corresponding to the arsenate phase, the peak at 461 cm^{-1} is of the SiO_2, the SiO_4 stretching doublet ~981 - 1040 cm^{-1} is characteristic of lead-alkali glaze, and the peak at 1601 cm^{-1} seems to be corresponding to the carbon (Colomban et al., 2017; Colomban et al., 2020; Colomban et al., 2022a).

2) Yellow

Opaque overglaze of bright yellow color is the component of polychromic painting at object 4 (**Figure 2(b)**). The pXRF testing was provided for the chrysanthemum flower's core (**Table 2**). Si, Al, and Pb are indicated as major elements. Minor elements are Sn, Fe, and Hf (**Table 3**). The combination of high lead and the presence of tin detects the lead-tin type of the overglaze. Raman spectrum taken at the chrysanthemum flower's core is presented in **Figure 4(c)**. The strongly shifted peak at 138 cm^{-1} is associated with the Pb-O component signaturing the lead-based pyrochlore yellow pigment. A peak around 800 - 810 cm^{-1} is interpreted as the signature of the arsenate phase. The peak at 463 cm^{-1} seems to be

associated with the Sn-O component (Miao et al., 2010; Colomban et al., 2020; Colomban et al., 2022a; Colomban et al., 2022b).

3) Green

Green overglazes of "warm" grass-green and "cold" emerald-green hues were examined at objects 4 and 9. Both are of translucent texture through which the drawn dark-colored leaves' veins are shining (**Figure 2(b)**, **Figure 2(c)**). Optical microscopy of object 9 in cross-section position shows that the layer of emerald-green overglaze is around 50 μm in thickness (**Figure 3(d)**).

The pXRF testing of two different greens at object 4 indicates that both are rich in Si and Pb, while Al, Cu, and Fe appear as minor elements. Cu content in "cold" green is 3.46 %wt. which is more than twice higher than 1.40 %wt. of Cu in "warm" green. The "warm" hue contains Sn as a minor element, and "cold" green contains Sb as a trace element (**Table 3**). At object 9, EDS spectra of the "cold" green area show SiO_2 and PbO as the majors and CuO and K_2O as the minors. In the area of "warm" green, major components are SiO_2, PbO, and SnO_2, and minor ones are CuO and K_2O. The CuO is about three times higher in "cold" green (**Table 4**). In general, the SEM-EDS and pXRF results are in agreement with each other, indicating that copper is a common element increasing in "cold" green and tin is the component of "warm" green. Under SEM, considered overglazes look different. In particular, the grass-green one is saturated with white shine particles corresponding to Sn inclusions (**Figure 5(a)**, **Figure 5(b)**).

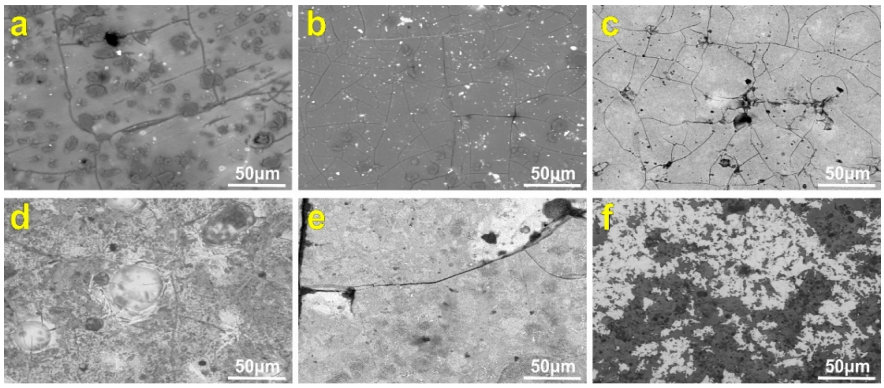

Figure 5. SEM micrographs of the overglazes. (a) object 9, emerald-green overglaze; (b) object 9, grass-green overglaze; (c) object 6, vermeil-red overglaze; (d) object 7, brown-black overglaze; (e) object 10, white overglaze; (f) object 6, gold overglaze.

4) Red

The overglaze of a "warm" terracotta-red hue is applied in painting and drawing techniques to objects 4, 5, and 8 (**Figure 2(b)**, **Figure 2(e)**; **Table 1**; **Table 2**). Object 5 was examined under an optical microscope in cross-section and surface positions at painted and drawn zones. The thickness of the red overglaze is around 50 - 60 μm (**Figure 3(e)**), and the texture looks coarse, with clearly visible dark-colored roundish grains (**Figure 3(h)**). According to research data, granular appearance under magnification is a distinctive characteristic of the paint subsist-

ence based on powdered hematite (Fe_2O_3) (Norris et al., 2020).

SEM-EDS detected PbO, SiO_2, and Fe_2O_3 as major components and Al_2O_3, K_2O, and CaO as the minor ones (**Table 4**). Raman spectroscopy applied to a dark part of the terracotta-red painted area at object 8 showed the shifted peaks at 223, 290, 406, and 1310 cm^{-1} (**Figure 4(d)**), indicating the hematite as a mineral phase of iron (Colomban et al., 2017; Colomban et al., 2020). Raman signatures of the hematite as peaks at 289, 477, and 602 cm^{-1}, and SiO_4 stretching band characteristic of lead-alkali enamel (doublet ~980 - 1049 cm^{-1}) are registered at object 4 (**Figure 5(e)**).

The overglaze of bright vermeil-red, or bloody-red, hue is applied in painting and drawing techniques on object 6 and for drawing on object 13. The optical microscopy of object 6 in surface position shows that red spots and contouring lines are overlapped by flaky gold paint, indicating the sequence of layers applying (**Figure 3(l)**). Under SEM, the characteristic microtextural trait is developed by crackling (**Figure 5(c)**). The EDS determined SiO_2, Fe_2O_3, and PbO as major components and K_2O, Na_2O, CaO, and CuO as constant minor ones. Copper seems to be a coloring agent that provides a bright, bloody shade. In some spectra, the Ag and Au are presented in minor concentrations caused by the penetrating from gold paint (**Table 4**).

5) Brown-black

A single case of dark brown-black overglaze is registered at object 7 where the composition of three standing vases with flowers is depicted. The wave-like figures of brown-black color are accented with thin gold strips (**Figure 2(d)**; **Table 2**). Under the optical microscope, the color looks dark brown with a purple shade. The texture looks uneven and grainy, similar to the texture of terracotta-red overglaze (**Figure 3(i)**). The SEM examination revealed crackling and developed bubbling at the micro level of the overglaze's texture (**Figure 5(d)**).

The EDS measured PbO, Fe_2O_3, and MnO in major concentrations. As researchers note, manganese provides purple or lavender shades (Norris et al., 2020). A distinctive feature of the composition is the presence of phosphorous and nitrogen in trace concentrations (**Table 4**). The result of the Raman examination is presented in **Figure 4(f)**. The doublet at 225 - 284 cm^{-1} and peak at 1307 cm^{-1} are corresponding to iron in the hematite phase, and peaks at 1350 cm^{-1} and 1587 cm^{-1} are associated with carbon. The peak at 609 cm^{-1} seems to be interpreted as the signature of Mn (Colomban et al., 2017; Colomban et al., 2020; Colomban et al., 2022b).

6) Violet-pink

The overglaze of this color is applied to the decoration of object 13. The thickness of the overglaze layer is around 80 μm, as optical microscopy of the cross-section shows (**Figure 3(f)**). The composition determined by SEM-EDS contains SiO_2 and PbO as the major, and Al_2O_3, Fe_2O_3, MnO, K_2O, CaO, and Na_2O as minor ones (**Table 4**). Manganese is considered a pigment that provides a specific lavender or violet shade.

7) Turquoise-blue

A single case of this overglaze is presented together with a violet-pink one at

object 13 (Table 1; Table 2). The color looks very delicate and quite distinctive of the intensive blue color at the objects 4, 7, 8, and 10. Optical microscopy of the surface position revealed a glassy texture with dark spots and crackles (Figure 3(j)). It is a strong bordering line between turquoise-blue and violet-pink overglazes (Figure 3(k)). The EDS examination detects high contents of PbO and SiO_2 as major components and As_2O_3, CuO, and K_2O as minor ones (Table 4).

8) White

At object 10, designed with floral motifs, the pink-colored flower's petals are accented by slicks of white opaque overglaze (Table 1; Table 2). Under SEM, the overglaze's texture looks relatively dense while having some crackles (Figure 5(e)). The composition of EDS spectra contains PbO and SiO_2 as major elements, As_2O_3 and K_2O as minor ones (Table 4).

9) Ruby-pink

The overglaze of this color, quite distinctive of the "warm" red hues considered above, is used in floral images painting at objects 10 and 11 (Figure 2(f); Table 2). Optical microscopy of the object 11 cross-section revealed a sequence of the body matrix, colorless glaze, and ruby-pink overglaze varying in thickness from 30 to 60 μm (Figure 3(g)). The overglaze composition was determined with the pXRF and EDS measuring at both objects and the same areas. The pXRF testing indicated the Au as a trace element and Pb as a major element in high content (Table 3). The EDS showed SiO_2 and PbO as the majors, Al_2O_3, K_2O, CaO, and N as the minors, and Fe as trace. Au was not indicated (Table 4).

10) Gold paint

The gold paint is identified on objects 5, 6, 7, and 8 (Table 1; Table 2). There are distinguished painting techniques and drawing, or lining, techniques of applying gold layer. Under optical microscopy, the gold layer shows a flaky and uneven texture contrasting with the compact glass-like texture of other overglazes (Figure 3(l)). The layer is extremely thin, ≤10 μm. Gold was painted over the fired glazed surface at objects 6 and 8 and lined over red and brown-black overglazes at objects 5 and 7 (Table 1; Table 2).

The pXRF testing of gold paint at object 6 indicated Au as the major element and Ag as the minor one. The P is registered as a major element (Table 3). An EDS examination of the gold area at object 6 detected the presence of Au as a major basic component. Another major component is Ag. An interesting feature is the constant presence of N in significant contents (Table 4). Under SEM, the light-colored and dark-colored areas are recognized in gold overglaze microtextural pattern (Figure 5(f)). The formers correspond to EDS spectra with high concentrations of Au but free of Pb, while dark-colored fields give the EDS signals of Au composing with Pb.

5. Discussion

Based on the archaeological and historical context of considered porcelain assemblage, the wares may be attributed, most likely, to the Yongzheng period (1723-

1735). This date is confirmed by the bottom trading mark on object 4 (**Figure 2(g)**).

The research results reflect some of the leading tendencies and fashions of Chinese porcelains' development during the early 18th century. In particular, the analysis illuminated specific technological features. The examined collection presents the cases of glaze, underglaze, overglaze, and gold painting treatments of porcelain. The composition of colorless transparent glaze at monochromic and polychromic objects corresponds to quartz-feldspar glazes with alkalis and lime contents (Colomban et al., 2022a). One common feature within the porcelain assemblage is that the colorless glaze layer is much thicker than both the colored underglaze and overglaze layers (**Figures 3(a)-(g)**). This observation is in agreement with the data on the porcelains of the 18th century: the thickness of colorless glaze lying on the body is circa 200 - 500 μm while the maximum thickness of the overglaze is circa 100 μm (Colomban et al., 2022a).

The case of object 3 decorated with an underglaze blue, is interesting in its distinctive spotted coloration (**Figure 2(a)**). Based on the external appearance, it seems to be possible to associate this fragmented ware with a relatively rare sort of Chinese porcelain known as *Powder Blue*, *Snowflake Blue*, or *Sprinkled Blue*, produced during the Kangxi and Yongzheng periods. Unusual "powdered" blue coloration combining dark and light areas was the result of the complicated technology of dispersing cobalt pigment over the unfired porcelain body with a special tube (Wilson & Watson, 1999: p. 102; Kelun, 2004: pp. 51, 52). The SEM-EDS and pXRF detect cobalt as a coloring agent of the underglaze in different concentrations in dark and light areas. The underglaze composition is characterized by high manganese content. The same feature is noted for blue underglazes of bottom marks on objects 4 and 6 (**Table 3**; **Table 4**). According to research data, the cobalt pigment used for examined underglazes is supposed to be the product of manganese-rich cobalt ores mined in China and other Asian regions in the early 18th century (Colomban et al., 2017; Giannini et al., 2017; Colomban et al., 2022c).

The external appearances and compositions of colorful overglazes, which are considered porcelains, correspond to the technological standards of the late Kangxi and Yongzheng periods. The observed textural features of examined overglazes are similar to those noted by the researchers. The referenced thickness of the overglazes is within the limits of 10 - 100 μm (Colomban et al., 2017; Colomban et al., 2022a). The crackles, spots, and bubbles at the overglaze surfaces under optical and electron microscopy are explained as the defects caused by the processes of firing and post-firing cooling (Norris et al., 2020; Colomban et al., 2022a).

All examined overglazes are of lead silicate composition with some contents of alkalis and calcium that is typical for Chinese overglazes (Norris et al., 2022). The highest contents of PbO, up to 34.5% - 37.1%, are registered in white and turquoise-blue overglazes, and most low ones in emerald-green, violet-pink, and vermeil-red overglazes. The alkalis as K_2O and Na_2O are more or less presented in all overglazes in minor and sometimes trace concentrations. Calcium is non-detected

in blue, grass-green, white, turquoise-blue, and ruby-pink overglazes (**Table 4**). The spectrum of detected coloring agents contains cobalt, iron, copper, tin, manganese, arsenic, and gold.

Blue overglazes examined on objects 7, 8, and 10 are cobalt-based and, in contrast to blue underglazes, poor in the manganese. Another remarkable trait is the arsenic indicated with the SEM-EDS as a minor element on object 10 and identified with the Raman on object 8. Based on the research data, the examined cases may be interpreted as evidence of the usage of European cobalt raw material rich in arsenic and poor in manganese. As known, since the late XVII century in Chinese porcelain production, a blue pigment made of cobalt ores imported from Europe was used for the overglaze decoration (Giannini et al., 2017; Norris et al., 2020; Colomban et al., 2022c; Norris et al., 2022).

The overglazes of terracotta-red, vermeil-red, and brown-black colors are iron-based. According to data from optical microscopy and Raman measuring, the hematite (Fe_2O_3) is indicated as a pigment. Iron-based overglazes, in particular with the hematite pigment, were used widely in Chinese porcelain production of the 18th century (Harrison-Hall, 1997; Colomban et al., 2017; Norris et al., 2020; Colomban et al., 2022a). In the brown-black overglaze on object 8 the combination of iron, manganese, and black carbon is detected. The same components are registered in dark-brown and brown-black Chinese overglazes (Colomban et al., 2020; Norris et al., 2020).

The green and yellow paintings represent copper-containing and tin-containing overglazes. The usage of transparent green overglazes of two or three hues of "warm" and "cold" spectra at the objects 4 and 9 is a distinctive trait of the *Famille Verte*, or *Kangxi Wucai*, porcelains introduced in the late Kangxi period (Harrison-Hall, 1997; Fang, 2010: pp. 100-105). Research data show that "warm" and "cold" green overglazes contain copper as a common chromophore, with a higher concentration in "cold" green. "Warm" or "light" hues are provided by the addition of tin in an overglaze composition (Norris et al., 2020; Norris et al., 2022). The results of our SEM-EDS and pXRF examination of emerald-green and grass-green overglazes correspond to these data. As for the composition of yellow overglaze at object 4 the results of pXRF and Raman examination allow us to suppose a Sn-rich variant of Naples yellow pyrochlore pigment of the European origin (Colomban et al., 2020).

The results of an examination of white and turquoise-blue overglazes detect that arsenic is a stable component. In Chinese porcelain production of the 18th century, arsenic was used widely as the opacifier producing non-transparent dense texture in white overglazes and adding soft pastel shades to the overglazes of turquoise-blue and some other colors (Harrison-Hall, 1997; Norris et al., 2020; Wang & Yang, 2022).

Ruby-pink overglaze examined on objects 10 and 11, which are fragmented small-sized cups and fine bowl-like ware, is characteristic of the famous Chinese *Famille Rose* porcelain introduced in the 1720s. The exquisite color was provided

by the addition of a small amount of colloidal gold to the composition (Harrison-Hall, 1997; Kerr & Wood, 2004: pp. 635-636; Colomban et al., 2017; Norris et al., 2020). The Au is detected in ruby-pink and overglazes at both noted objects using the pXRF but is not recognized with the SEM-EDS.

The research data highlights that the EDS analysis is not efficient for identifying small amounts of Au in the lead-containing overglazes, so other methods are recommended, in particular, the XRF analysis (Norris et al., 2022). It is noteworthy that SEM-EDS and pXRF measurements did not detect Sn in certain overglazes, even in trace amounts. As some researchers note, the presence of tin suggests that the European origin of ruby-pink overglaze composition, while the absence of tin, on the contrary, indicates independent Chinese receipt (Norris et al., 2020). Note that at object 10, a ruby-pink overglaze is used together with a cobalt-containing blue overglaze that is free of manganese. This observation is in good agreement with research data on the imported European cobalt-based blue overglazes used in the decoration of *Famille Rose* porcelain (Giannini et al., 2017).

As a result, we suppose that some famous sorts of porcelains of the early 18th are presented in considered assemblage—the *Powder Blue*, *Snowflake Blue*, or *Sprinkled Blue* as object 3, the *Famille Verte* as object 4 and, preliminary, object 9, and the *Famille Rose* as the objects 10 and 11.

The technology of gilding is identified on objects 5 - 8 in two variants—gold paint overfired glaze (objects 6, 8) and gold paint overfired overglaze (objects 5, 7). The researchers note that gold paint was usually applied over fired overglazes and glazes and then was processed at low temperatures, 600˚C - 800˚C (Kerr & Wood, 2004: p. 697; Norris et al., 2022). SEM-EDS and pXRF data correspond to each other in the detection of high Au and relatively low Ag in gold paint. This correlates with known research data on the compositions of gold paints of Chinese porcelains and enameled metals in the 18th century (Norris et al., 2020; Norris et al., 2022; Colomban et al., 2022a).

In China, the technology of ceramic object gilding was initiated in the Tang dynasty period (609 - 907) and developed in relation to metal object gilding. Chinese craftsmen used seven different technological receipts of gilding, but the gold painting, in particular, of the porcelains of early18th, was not always of satisfactory quality and was especially important for the export, European-oriented production (Kerr & Wood, 2004: pp. 700-702). In Europe, the technology of gilding decoration has its own history and achievements. As known, in France, the mixing of gold powder with some organic components like honey, egg white, gum Arabic, and garlic oil was used in enameling techniques for better adhesion and attractive-looking gilding decoration (Hunt, 1979; Kerr & Wood, 2004: p. 703; Manners, 2011). In this connection, it is interesting to note high contents of the phosphorous detected by the pXRF and nitrogen detected by SEM-EDS in the gold painting composition at examined object 6—a fine plate decorated with bright gold flowers and stamped at the bottom with the *Pi ting ju'i* mark (**Table 1**; **Figure 2**). High concentrations of P and N are not recognized in other overglazes and glazes

in the studied specimens. This is a reason to think that in the case of object 6, the phosphorous and nitrogen are not the soil pollutions but the indicators of some initial organic components of the gold paint composition. Supposedly, object 6 represents the case of the usage of gold paint receipt influenced by European technologies. It looks not surprising, taking into account the active development of the contacts and interrelations in fine arts and crafts between imperial China and European countries in the late 17th and early 18th centuries (Fang, 2010: pp. 106-109; Giannini et al., 2017; Norris et al., 2022; Colomban et al., 2022a).

Completing the Discussion section, some short remarks on the artistic features of considered porcelains may be added. Most of the examined objects are decorated with colorful overglazed paintings, but their fragmentary origin significantly limits our observations on picturing themes, images, and motifs. At objects 4 - 6 and 9 - 11, various images of wildlife are recognized, such as flowers, leaves and stems, and butterflies. Object 4 is a fine saucer dish, and objects 9 and 11, as fragments of small bowls, demonstrate pastel and vibrant appearance of colors similar to true painting art (**Figure 2(b)**, **Figure 2(c)**, **Figure 2(f)**). This outstanding level of paint decoration was achieved in Chinese porcelain production in the early 18th century, especially in the Yongzheng period (Fang, 2010: pp. 106-107; Wang & Yang, 2022). It may be noted that the theme of flowers and butterflies presented in object 4 was used widely in the painting of porcelains produced in Jingdezhen's imperial workshops (Harrison-Hall, 1997). The compositions of interlocking flowers and leaves decorate plate-shaped objects 5 and 6 (**Table 1**), but color schemes differ from objects 4 and 11. Object 5's bright polychromic pattern lacks an attractive pastel appearance with tender shades. Object 6: flashy gold paint provides a main decorative effect.

Objects 7 and 8, as fragmented small plates, represent painted compositions that seem to be inspired by traditional Chinese beliefs and auspicious symbolism. At object 7 the vases or containers with flowers are depicted as a well-known symbol of harmony and peace (**Figure 2(d)**). Object 8, a preserved fragment of the painting, looks like an installation composed of a large rectangular-legged container looking like burned incense, a pair of golden, intricately shaped vessels, and the object like a stringed musical instrument (**Figure 2(e)**). The trend to use in porcelain painting various symbolic images and spiritual meanings emerging in the late Kangxi period became especially popular in the Yongzheng period (Fang, 2010: pp. 105, 115). The manner of the referenced plates' decoration looks slightly careless and rough in contrast to elegant and refined patterns at objects 4 and 9, representing the *Famille Verte* and the *Famille Rose* porcelains.

Based on the data referenced in Section 2, we consider the porcelain assemblage discovered at the Vitus Bering campsite as export Chinese production traded to Russia in the early 18th century. Technological and artistic features indicate different styles and qualities of the porcelains. Supposedly, these were the products of different kilns and workshops. As known, in the late Kangxi period and Yongzheng period, due to great activity of the export trading, not only Imperial kilns in Jing-

dezhen but a large amount of commoner, or folk, kilns were involved in the production of porcelains (Fang, 2010: pp. 103, 137; Wang & Yang, 2022).

6. Conclusion

As the researchers note, Chinese porcelain wares of the early 18th century, and in particular, of the Yongzheng period (1723-1735), are quite rare and, therefore, interesting for special studies (Norris et al., 2020). Based on the archaeometry approach that provides technological insights, the porcelain assemblage from the remains of Vitus Bering's campsite at the Commander Islands is determined to be Chinese production. Considered specimens certainly reflect some trends and developments of Chinese porcelain during the late Kangxi (1662-1722) and Yongzheng periods. Thus, the *Famille Rose* and *Famille Verte* overglazed porcelains, *Powdered Blue* underglaze porcelain, and the porcelains decorated with gold are recognized. These prestigious and expensive sorts of Chinese porcelain tableware, in particular, exported production, are supposed to be among the personnel belongings of Great Northern Expedition (1733-1742) members, indicating the process of entering the Chinese porcelain of early 18th century into the European and Russian everyday culture. As a whole, the findings from the Vitus Bering camp site contribute to our knowledge about global trading and the spreading of Chinese porcelain in the first half of the 18th century.

Acknowledgements

The authors cordially thank Prof. Peter Jordan for his kind assistance in improving the English language of this article.

Conflicts of Interest

The authors declare no conflicts of interest regarding the publication of this paper.

References

Burton, W., & Hobson, R. L. (1909). *Handbook of Marks on Pottery & Porcelain*. Macmillan and Co., Limited. https://doi.org/10.5479/sil.181102.39088000024257

Colomban, P., Ambrosi, F., Ngo, A., Lu, T., Feng, X., Chen, S. et al. (2017). Comparative Analysis of Wucai Chinese Porcelains Using Mobile and Fixed Raman Microspectrometers. *Ceramics International, 43,* 14244-14256. https://doi.org/10.1016/j.ceramint.2017.07.172

Colomban, P., Gironda, M., Simsek Franci, G., & d'Abrigeon, P. (2022a). Distinguishing Genuine Imperial Qing Dynasty Porcelain from Ancient Replicas by On-Site Non-Invasive XRF and Raman Spectroscopy. *Materials, 15,* Article 5747. https://doi.org/10.3390/ma15165747

Colomban, P., Kırmızı, B., Zhao, B., Clais, J., Yang, Y., & Droguet, V. (2020). Investigation of the Pigments and Glassy Matrix of Painted Enamelled Qing Dynasty Chinese Porcelains by Noninvasive On-Site Raman Microspectrometry. *Heritage, 3,* 915-940. https://doi.org/10.3390/heritage3030050

Colomban, P., Ngo, A., & Fournery, N. (2022b). Non-Invasive Raman Analysis of 18th Century Chinese Export/Armorial Overglazed Porcelain: Identification of the Different

Enameling Techniques. *Heritage, 5,* 233-259. https://doi.org/10.3390/heritage5010013

Colomban, P., Simsek Franci, G., Burlot, J., Gallet, X., Zhao, B., & Clais, J. (2023). Non-Invasive On-Site pXRF Analysis of Coloring Agents, Marks and Enamels of Qing Imperial and Non-Imperial Porcelain. *Ceramics, 6,* 447-474. https://doi.org/10.3390/ceramics6010026

Colomban, P., Simsek Franci, G., Gironda, M., d'Abrigeon, P., & Schumacher, A. (2022c). pXRF Data Evaluation Methodology for On-Site Analysis of Precious Artifacts: Cobalt Used in the Blue Decoration of Qing Dynasty Overglazed Porcelain Enameled at Customs District (Guangzhou), Jingdezhen and Zaobanchu (Beijing) Workshops. *Heritage, 5,* 1752-1778. https://doi.org/10.3390/heritage5030091

Fang, L. (2010). *Chinese Ceramics: A History of Elegance*. China Intercontinental Publishing.

Giannini, R., Freestone, I. C., & Shortland, A. J. (2017). European Cobalt Sources Identified in the Production of Chinese *famille rose* Porcelain. *Journal of Archaeological Science, 80,* 27-36. https://doi.org/10.1016/j.jas.2017.01.011

Harrison-Hall, J. (1997). Chinese Porcelain from Jingdezhen. In I. Freestone, & D. Gaimster (Eds.), *Pottery in the Making: World Ceramic Traditions* (pp. 194-199). British Museum Press.

Huang, Z. (2019). The Development and Change of Kyakhta Trade in the 18th and 19th Centuries. *Advances in Historical Studies, 8,* 131-137. https://doi.org/10.4236/ahs.2019.83010

Hunt, L. B. (1979). Gold in the Pottery Industry: The History and Technology of Gilding Processes. *Gold Bulletin, 12,* 116-127. https://doi.org/10.1007/bf03215112

Kelun, C. (2004). *Chinese Porcelain: Art, Elegance, and Appreciation (Arts of China)*. Long River Publishing.

Kerr, R., & Wood N. (2004). *Science and Civilization in China. Vol. 5. Chemistry and Chemical Technology, Part XII: Ceramic Technology*. Cambridge University Press.

Leath, R. A. (1999). "After the Chinese Taste": Chinese Export Porcelain and Chinoiserie Design in Eighteen-Century Charleston. *Historical Archaeology, 33,* 48-61. https://doi.org/10.1007/bf03373622

Len'kov, V. D., Silant'ev, G. L., & Staniukovich, A. K. (1988). *Komandorskii lager' ek-speditsii Beringa (Opyt kompleksnogo izucheniia)*. Nauka Publishing.

Len'kov, V. D., Silant'ev, G. L., & Staniukovich, A. K. (1992). *The Komandorskii Camp of Bering Expedition: An Experiment in Complex Study*. The Alaska Historical Society Publishing.

Manners, E. (2011). Gold Decoration on French, German, and Oriental Porcelain in the Early 18th Century. *Journal of The French Porcelain Society, 4,* 24-42.

Miao, J., Yang, B., & Mu, D. (2010). Identification and Differentiation of Opaque Chinese Overglaze Yellow Enamels by Raman Spectroscopy and Supporting Techniques. *Archaeometry, 52,* 146-155. https://doi.org/10.1111/j.1475-4754.2009.00466.x

Norris, D., Braekmans, D., & Shortland, A. (2022). Technological Connections in the Development of 18th and 19th Century Chinese Painted Enamels. *Journal of Archaeological Science: Reports, 42,* Article 103406. https://doi.org/10.1016/j.jasrep.2022.103406

Norris, D., Braekmans, D., Domoney, K., & Shortland, A. (2020). The Composition and Technology of Polychrome Enamels on Chinese Ruby-Backed Plates Identified Through Nondestructive Micro-X-Ray Fluorescence. *X-Ray Spectrometry, 49,* 502-510. https://doi.org/10.1002/xrs.3144

Tataurov, F. S. (2017). Chinese Porcelain from Russian Sites of the Middle Irtysh in 17th—First Half of the 18th Centuries. In S. Bocharov, V. François, & A. Sitdikov (Eds.), *Glazed Pottery of the Mediterranian and the Black Sea Region, 10th-18th Centuries.* (Vol. 2, pp. 835-842). Stratum Plus Press.

Wang, C., & Yang, X. (2022). Exploring the Visual Beauty of Pastel Porcelain in Qing Dynasty. *Art and Performance Letters, 3,* 10-14.

Wilson, G., & Watson, F. (1999). *Mounted Oriental Porcelain in the J. Paul Getty Museum*. Paul Getty Museum Publishing.

Zagvazdina, Y. G. (2017). Finds of Chinese Porcelain from the Cultural Layer of Tobolsk. In L. V. Tataurova (Ed.), *Culture of Russians in Archaeological Researches* (pp. 463-465). Nauka Publishing.